



HAL
open science

Endoplasmic reticulum maintains ion homeostasis required for plasma membrane repair

Goutam Chandra, Sen Chandra Sreetama, Davi A.G. Mázala, Karine Charton, Jack H Vandermeulen, Isabelle Richard, Jyoti K Jaiswal

► **To cite this version:**

Goutam Chandra, Sen Chandra Sreetama, Davi A.G. Mázala, Karine Charton, Jack H Vandermeulen, et al.. Endoplasmic reticulum maintains ion homeostasis required for plasma membrane repair. *Journal of Cell Biology*, 2021, 220 (5), 10.1083/jcb.202006035 . hal-03358287

HAL Id: hal-03358287

<https://univ-evry.hal.science/hal-03358287>

Submitted on 29 Sep 2021

HAL is a multi-disciplinary open access archive for the deposit and dissemination of scientific research documents, whether they are published or not. The documents may come from teaching and research institutions in France or abroad, or from public or private research centers.

L'archive ouverte pluridisciplinaire **HAL**, est destinée au dépôt et à la diffusion de documents scientifiques de niveau recherche, publiés ou non, émanant des établissements d'enseignement et de recherche français ou étrangers, des laboratoires publics ou privés.

REPORT

Endoplasmic reticulum maintains ion homeostasis required for plasma membrane repair

Goutam Chandra¹, Sen Chandra Sreetama¹, Davi A.G. Mázala¹, Karine Charton² , Jack H. VanderMeulen¹, Isabelle Richard² , and Jyoti K. Jaiswal^{1,3} 

Of the many crucial functions of the ER, homeostasis of physiological calcium increase is critical for signaling. Plasma membrane (PM) injury causes a pathological calcium influx. Here, we show that the ER helps clear this surge in cytoplasmic calcium through an ER-resident calcium pump, SERCA, and a calcium-activated ion channel, Anoctamin 5 (ANO5). SERCA imports calcium into the ER, and ANO5 supports this by maintaining electroneutrality of the ER lumen through anion import. Preventing either of these transporter activities causes cytosolic calcium overload and disrupts PM repair (PMR). ANO5 deficit in limb girdle muscular dystrophy 2L (LGMD2L) patient cells compromises their cytosolic and ER calcium homeostasis. By generating a mouse model of LGMD2L, we find that PM injury causes cytosolic calcium overload and compromises the ability of ANO5-deficient myofibers to repair. Addressing calcium overload in ANO5-deficient myofibers enables them to repair, supporting the requirement of the ER in calcium homeostasis in injured cells and facilitating PMR.

Introduction

There is an ~1,000-fold calcium (Ca²⁺) gradient across the plasma membrane (PM), which is maintained by the barrier function of the PM and by pumping Ca²⁺ into the extracellular space or intracellular compartments (Jaiswal, 2001; McNeil and Steinhardt, 2003). PM injury disrupts this gradient, causing a large and rapid influx of extracellular Ca²⁺, which triggers the PM repair (PMR) response (Cooper and McNeil, 2015; Horn and Jaiswal, 2018; McNeil and Steinhardt, 2003). How cells undergoing repair buffer this cytosolic Ca²⁺ ([Ca²⁺]_c) excess and how failure to do so affects PMR have not been resolved.

The ER, which constitutes ~50% of the eukaryotic cell's membrane, is the major reservoir for intracellular calcium. While the resting [Ca²⁺]_c is ~100 nM, sarco/endoplasmic reticulum Ca²⁺-ATPase (SERCA) pumps [Ca²⁺]_c into the ER and maintains free Ca²⁺ concentration in the ER ([Ca²⁺]_{ER}) in the range of 100 to 400 μM (Palmer et al., 2006; Samtleben et al., 2013; Verkhatsky, 2005). This Ca²⁺ is a required cofactor for the ER-resident chaperones to maintain their optimal activity. ER Ca²⁺ homeostasis is essential for a variety of functions, including cell signaling, immune cell development and function, and muscle cell contraction. However, whether the ER plays a role in homeostasis of PM injury-triggered increase in cellular Ca²⁺ and its role in PMR have not been investigated. For the ER to play a role in [Ca²⁺]_c buffering, it must sense the increase in [Ca²⁺]_c and

buffer it by rapidly sequestering it. SERCA, the pump responsible for Ca²⁺ import into the ER, binds Ca²⁺ for its import. However, instead of [Ca²⁺]_c level, SERCA pump is regulated by the binding of multiple small-molecular-weight proteins such as sarcolipin and phospholamban (Chen et al., 2020; Stammers et al., 2015). Ca²⁺ pumping into the ER by SERCA is kept electroneutral through the exchange of imported Ca²⁺ with exported H⁺ (Møller et al., 2010) and transport of counter-ions such as Chloride (Cl⁻) into the ER is required to maintain electroneutrality during uptake of large Ca²⁺ influx (Pollock et al., 1998). Large [Ca²⁺]_c surge, such as that caused by purinergic signaling, enables Ca²⁺ import into the ER by calcium-activated chloride channel (CaCC)-mediated Cl⁻ uptake into the ER (Neussert et al., 2010).

The transmembrane protein 16 (TMEM16) family, also known as the Anoctamin (ANO) family of proteins, includes calcium-activated anion channels (Berg et al., 2012; Huang et al., 2012; Whitlock and Hartzell, 2017). ANO5 (TMEM16E), a member of this family that is proposed to be a nonselective ion channel, localizes to the ER and is required for PMR (Di Zanni et al., 2018; Griffin et al., 2016; Jaiswal et al., 2007; Tsutsumi et al., 2004). Thus, lack of ANO5 may disrupt rapid electro-neutral exchange of Ca²⁺ required for ER Ca²⁺ homeostasis. However, ANO5 function has not been examined at the ER, and

¹Center of Genetic Medicine Research, Children's National Health System, Washington, DC; ²Généthon, Institut National de la Santé et de la Recherche Médicale, U951, INTEGRARE Research Unit, University Paris-Saclay, Evry, France; ³Department of Genomics and Precision Medicine, George Washington University School of Medicine and Health Sciences, Washington, DC.

Correspondence to Jyoti K. Jaiswal: jkjaiswal@cnmc.org.

© 2021 Chandra et al. This article is distributed under the terms of an Attribution–Noncommercial–Share Alike–No Mirror Sites license for the first six months after the publication date (see <http://www.rupress.org/terms/>). After six months it is available under a Creative Commons License (Attribution–Noncommercial–Share Alike 4.0 International license, as described at <https://creativecommons.org/licenses/by-nc-sa/4.0/>).

much of the analyses have focused on its activity at the PM (Di Zanni et al., 2020; Di Zanni et al., 2018; Duran et al., 2012). Recessive mutations in the *ANO5* gene are associated with limb girdle muscular dystrophy 2L (LGMD2L) and Miyoshi muscular dystrophy 3, characterized by progressive muscle weakness and degeneration (Hicks et al., 2011; Sarkozy et al., 2013; Witting et al., 2013). Defects in PMR are also associated with muscle diseases including, LGMD2B, LGMD2D, Facioscapulohumeral muscular dystrophy, and Duchenne muscular dystrophy, where PMR deficit is linked to altered membrane trafficking and mitochondrial redox signaling (Bansal et al., 2003; Bittel et al., 2020; Defour et al., 2014b; Han et al., 2009; Vila et al., 2017). However, cells from muscular dystrophy patients with *ANO5* mutations (Bolduc et al., 2010) show poor PMR even when the conventional PMR pathways are unaffected (Chandra et al., 2019; Jaiswal et al., 2007). Despite over a dozen unique *ANO5* mutations identified, the exact mechanism for poor PMR in *ANO5*-deficient cells has not been established (Penttilä et al., 2012).

Here, we studied Ca^{2+} dynamics during the repair of injured cells and the role of CaCC in regulating this homeostasis. Our work examines whether the ER helps regulate Ca^{2+} homeostasis following PM injury and the consequence of failure to buffer $[\text{Ca}^{2+}]_c$ excess caused by PM injury. We also examined whether ER-mediated calcium homeostasis plays a role in the repair of *ANO5*-deficient cells. To examine these, we made use of *ANO5* patient muscle cells as well as a new *ANO5* knockout (KO) mouse model. Our studies with healthy cells identify that CaCC-mediated chloride uptake by the ER is required for PMR and that this is compromised in muscle cells of *ANO5*-deficient patient, as well as in myofibers of *ANO5*-KO mice. This deficit in $[\text{Ca}^{2+}]_c$ clearance results in ER and mitochondrial damage due to Ca^{2+} overload, the reversal of which restores PMR ability in *ANO5*-deficient cells. These findings identify a novel role of the ER in cell survival, shows that regulation of Ca^{2+} homeostasis is a key step in the process of PMR, and provides mechanistic insight into the basis for PMR deficit in LGMD2L/Miyoshi muscular dystrophy 3 patient muscles.

Results

The ER facilitates PMR by buffering an injury-triggered increase in $[\text{Ca}^{2+}]_c$

Using the free Ca^{2+} -sensor Fluo-4, we monitored the change in $[\text{Ca}^{2+}]_c$ during PMR in healthy human myoblasts. Focal PM injury caused influx of extracellular Ca^{2+} , which caused the $[\text{Ca}^{2+}]_c$ to peak in 6.06 ± 0.45 s, which returned to baseline in 39.52 ± 5.13 s (Fig. 1, A and B). Use of membrane-impermeant FM1-43 dye entry into cells as an indicator of PMR showed that $[\text{Ca}^{2+}]_c$ influx returns to near baseline as the PM wound closes by 40 s. This leads to the plateauing of FM dye entry, but this cessation of FM dye entry fails to occur when cells are injured in the absence of extracellular Ca^{2+} (Fig. 1, C and D). Thus, PM wound closure requires extracellular Ca^{2+} entry to trigger repair, but this Ca^{2+} is rapidly buffered by an as-yet-unknown mechanism. Because the ER is the major intracellular store for Ca^{2+} , we examined whether it helps buffer the injury-triggered increase in $[\text{Ca}^{2+}]_c$. For this, we used the Förster (fluorescence) resonance energy

transfer (FRET)-based ER luminal Ca^{2+} sensor (T1ER; Abell et al., 2011). Following PM injury, ER Ca^{2+} levels increased immediately (Fig. 1, F and G), with the fastest increase occurring during the first 30 s of injury, the period when the $[\text{Ca}^{2+}]_c$ increase was buffered most rapidly (Fig. 1 B). To test whether ER Ca^{2+} uptake helps buffer the injury-triggered increase in $[\text{Ca}^{2+}]_c$, we blocked ER Ca^{2+} uptake using the SERCA pump inhibitor thapsigargin (TG; Fig. 1, H and G). This prevented the injury-triggered increase in $[\text{Ca}^{2+}]_c$ from returning to baseline (Fig. 1, B and I). Blocking the ER uptake of Ca^{2+} prevented PMR, as indicated by continued FM1-43 dye entry in TG-treated injured cells (Fig. 1, D and J), and reduced the number of injured cells managing to undergo PMR (Fig. 1 E). While signal-triggered Ca^{2+} release from the ER is well studied, this is not so for the mechanism of $[\text{Ca}^{2+}]_c$ -activated Ca^{2+} uptake by the ER.

Counter-ion transport is required for ER Ca^{2+} uptake during PMR

While the SERCA pump is not sensitive to the $[\text{Ca}^{2+}]_c$ level, import of counter ions such as Cl^- into the ER maintains electroneutrality during uptake of large Ca^{2+} influx (Pollock et al., 1998). Ca^{2+} sensitivity of counter-ion import is due to CaCCs (Neusser et al., 2010). To investigate whether this mechanism enables ER Ca^{2+} uptake during PMR, we inhibited CaCCs using 5-nitro-2-(3-phenylpropyl-amino) benzoic acid (NPPB; Dreinhöfer et al., 1988). To monitor NPPB-blocked anion entry into the ER, we used the anion sensitivity of YFP (Kuner and Augustine, 2000). ER-localized YFP (YFP_{ER}) and RFP (RFP_{ER}) were expressed in cells and treated with NPPB or vehicle (DMSO). PM injury of vehicle-treated cells led to anion uptake-induced rapid quenching of YFP_{ER} fluorescence, decreasing the $\text{YFP}_{\text{ER}}/\text{RFP}_{\text{ER}}$ ratio (Fig. 2, A and B; and Fig. S2). As expected, this was prevented in NPPB-treated cells (Fig. 2, A and B), identifying that NPPB-sensitive Ca^{2+} -activated anion channels enable injury-triggered anion influx into the ER. Use of T1ER showed that NPPB treatment also prevented the injury-induced increase in $[\text{Ca}^{2+}]_{\text{ER}}$ (Fig. 2, C and D). This NPPB-induced block in $[\text{Ca}^{2+}]_{\text{ER}}$ increase prevented the buffering of the injury-triggered increase in the $[\text{Ca}^{2+}]_c$ (Fig. 2, E and F). NPPB treatment led to a dose-dependent decrease in PMR, as shown by increased FM1-43 dye entry and a decrease in the number of cells that underwent PMR (Fig. 2, G–I). These results suggest that CaCC activity allows Ca^{2+} uptake by the ER and is required for PMR.

ANO5 deficit impairs $[\text{Ca}^{2+}]_{\text{ER}}$ homeostasis and prevents PMR by $[\text{Ca}^{2+}]_c$ overload

KO of the ANO family member *ANO5* (*TMEM16E*) and cells from patients with mutations in *ANO5* both exhibit poor PMR (Chandra et al., 2019; Griffin et al., 2016; Jaiswal et al., 2007). To examine if injured *ANO5* patient fibroblasts exhibit altered ER Ca^{2+} homeostasis, we monitored $[\text{Ca}^{2+}]_{\text{ER}}$ following injury. This showed significantly reduced $[\text{Ca}^{2+}]_{\text{ER}}$ in injured patient fibroblasts (Fig. S1, A and B). As lack of CaCC in the ER has been shown to affect ER calcium homeostasis during purinergic signaling (Neusser et al., 2010), we treated patient cells with ATP (50 μM) and found that unlike the healthy cells, ATP failed to increase in $[\text{Ca}^{2+}]_{\text{ER}}$ in patient cells (Fig. S1, C and D). Similar to

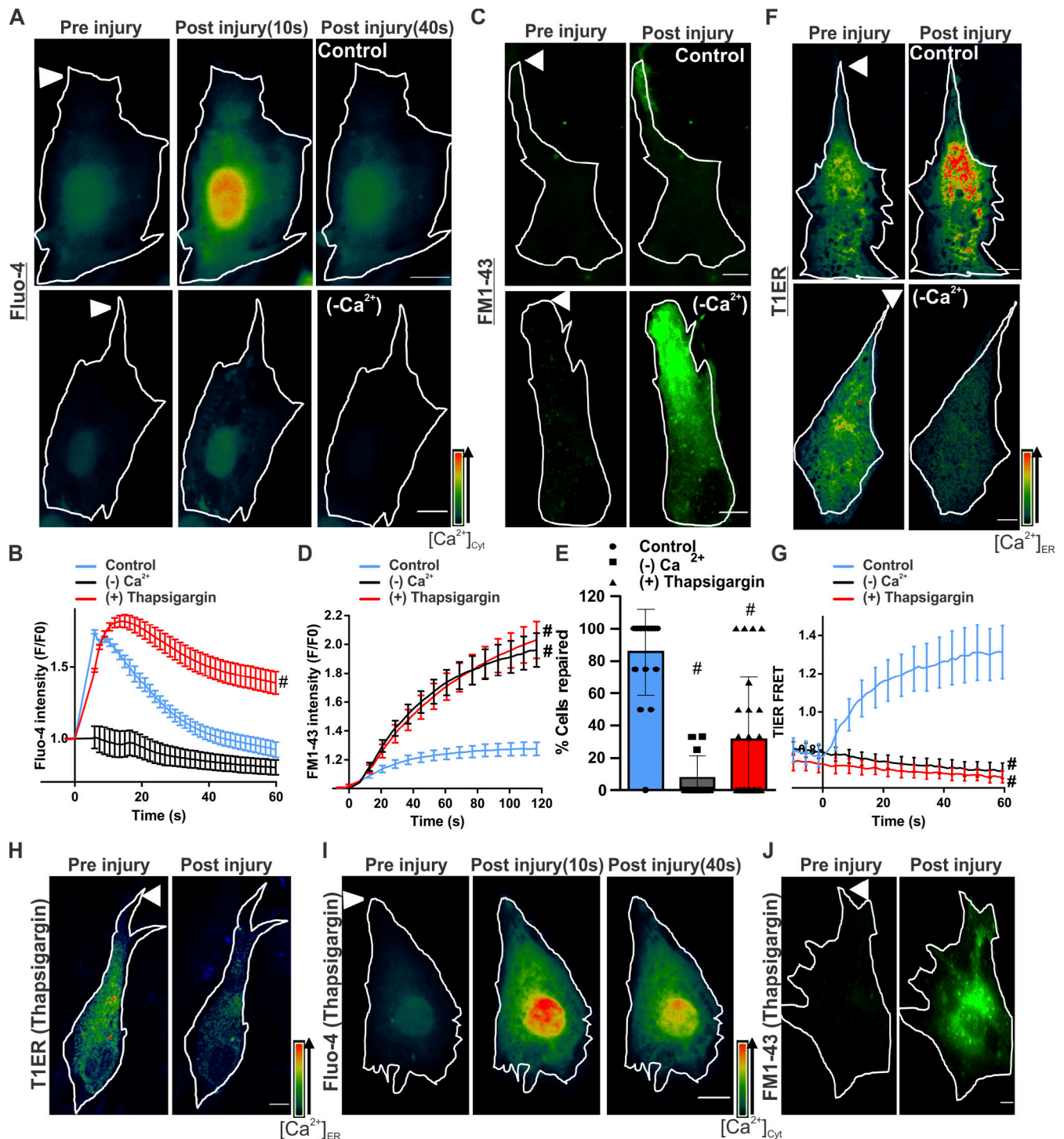


Figure 1. [Ca²⁺]_c homeostasis is required for PMR. (A) Healthy human myoblasts were labeled with Fluo-4 to monitor [Ca²⁺]_c following focal PM injury (arrowheads) by laser in the presence (control) or absence (-Ca²⁺) of extracellular Ca²⁺. Pseudocolored images of the cell at different time points before and following injury are shown. Injury sites are marked with arrowheads. (B) Quantification of averaged kinetics for Fluo-4 intensity change in cells injured in the presence (control) or absence (-Ca²⁺) of extracellular Ca²⁺ or in the presence of SERCA inhibitor (1 mM TG). Plot shows mean ± SEM. *n* = 33 (control), 19 (-Ca²⁺) and 29 (TG) cells; #, *P* < 0.0001. (C) Images showing FM1-43 dye entry into human myoblasts before and 60 s after focal laser injury in the presence (control) or absence (-Ca²⁺) of extracellular Ca²⁺. (D) Quantification of FM1-43 dye entry kinetics in healthy myoblasts in the presence or absence of extracellular Ca²⁺ or treated with 1mM TG in presence of Ca²⁺. Plot shows mean ± SEM. *n* = 16 (control), 25 (-Ca²⁺) and 16 (TG) cells.; #, *P* < 0.0001. (E) Percentage of cells in C and D that successfully repaired. Plot shows mean ± SD. #, *P* < 0.0001. (F) Images before and 60 s after injury of human myoblasts expressing FRET-based ER calcium sensor T1ER, injured with (control) or without (-Ca²⁺) extracellular Ca²⁺. (G) Quantification of normalized T1ER FRET ratios in cells injured as indicated. Plot shows mean ± SEM. *n* = 20 (control), 9 (-Ca²⁺) and 17 cells (TG); #, *P* < 0.0001. (H-J) Images of human myoblasts labeled with T1ER (H), Fluo-4 (I), and FM1-43 (J) and treated with TG (1 mM) to inhibit SERCA. Images show the same cell before (preinjury) and 60 s (or indicated time points) after injury. Scale bars, 10 μm. Arrowhead indicates site of laser injury.

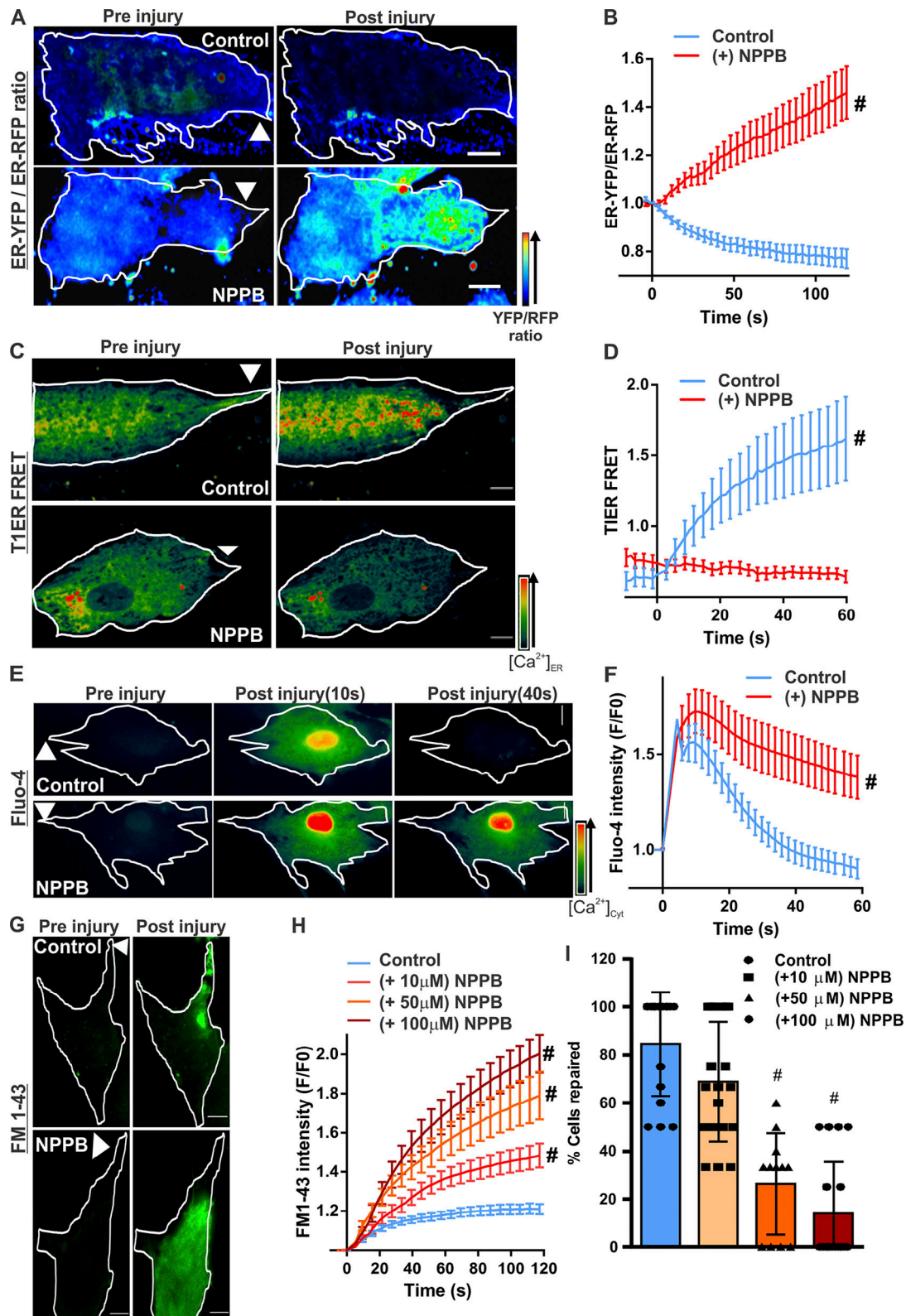


Figure 2. **Ca²⁺ homeostasis during PMR requires CaCC activity.** Human myoblasts expressing KDEL-YFP and KDEL-RFP were treated with vehicle (control) or a CaCC blocker (50 μ M NPPB). Quenching of YFP fluorescence by Cl⁻ entry into the ER was monitored by ratiometric measurement of Cl⁻-sensitive YFP and Cl⁻-insensitive RFP fluorescence. **(A)** Pseudocolored images of cells before or 60s after laser injury (injury site marked by arrowheads). **(B)** Quantification of the normalized YFP/RFP ratio in control and NPPB-treated myoblasts. *n* = 18 (control) and 16 (NPPB) cells; #, *P* < 0.0001. **(C and D)** Pseudocolored images (C) and quantification (D) of T1ER FRET ratios before and after injury of myoblasts treated with vehicle (control) or NPPB (50 μ M). Arrowheads indicate site of injury. *n* = 20 (control) and 17 (NPPB 50 μ M) cells; #, *P* < 0.0001. **(E and F)** Pseudocolored images (E) and plots (F) showing change in $[Ca^{2+}]_c$ monitored by Fluo-4

labeling of human myoblasts treated with vehicle (control) or NPPB. $n = 23$ (control) and 24 (NPPB) cells; #, $P < 0.0001$. **(G and H)** Images (G) and plots (H) showing FM1-43 dye entry into healthy myoblasts treated with vehicle (control) or NPPB (at indicated doses) and focally injured by laser (site marked with arrowheads). **(I)** Percentage of myoblasts that repaired from PM injury after treatment with indicated NPPB doses. $n = 16$ (control), 19 (NPPB 10 μM), 12 (NPPB 50 μM), and 18 (NPPB 100 μM) cells; #, $P < 0.0001$. Error bars represent SD for the plot in I and SEM for all other plots. Scale bars, 10 μm .

fibroblasts, the $\text{YFP}_{\text{ER}}/\text{RFP}_{\text{ER}}$ ratio in injured healthy human myoblasts decreased, indicating anion influx in the ER, and this was blocked in ANO5 patient myoblasts (Fig. 3, A and B; and Fig. S2). Using T1ER, we found that the block in ER anion uptake in patient cells occurred concomitantly with the block in ER Ca^{2+} uptake in patient cells (Fig. 3, C and D). Further, failure of ER Ca^{2+} uptake by injured patient cells correlated with their poor PMR (Fig. 3, E–G). To confirm if failure of ER calcium uptake compromises PMR of patient cells, we examined whether SERCA inhibition (by TG) can worsen the PMR deficit in patient cells. While TG impaired PMR of healthy cells, it did not worsen the repair deficit of patient cells (Fig. 3, E–G). Together, these results indicate that lack of ANO5 prevents PMR by preventing the ER counter-ion influx required for cytosolic $[\text{Ca}^{2+}]_{\text{c}}$ buffering during PMR.

To determine why failed $[\text{Ca}^{2+}]_{\text{c}}$ buffering compromises PMR, we examined whether poor buffering of $[\text{Ca}^{2+}]_{\text{c}}$ disrupts normal PMR responses. Annexins are among the earliest cytoplasmic proteins that respond to injury-triggered $[\text{Ca}^{2+}]_{\text{c}}$ increase, and their strict temporal response is required for successful PMR (Demonbreun et al., 2016; Jaiswal et al., 2014; Jaiswal and Nylandsted, 2015; Sønder et al., 2019). We monitored the response of annexin A1 and A2, both of which are implicated in PMR. Both annexins accumulated immediately upon PM injury and cleared within 1 min of injury in healthy cells (Fig. 3, H–J). However, in patient cells, both annexins continued to accumulate for longer, accumulated to a higher level, and failed to clear away from the injury site (Fig. 3, H–J). This demonstrates that poor $[\text{Ca}^{2+}]_{\text{c}}$ buffering in injured patient cells disrupts the timely PMR response by annexins.

Another response triggered by injury-induced increase in Ca^{2+} is mitochondria-mediated PMR (Horn and Jaiswal, 2018; Horn et al., 2020; Horn et al., 2017; Sharma et al., 2012). To examine this response in ANO5-deficient cells, we used the $[\text{Ca}^{2+}]_{\text{m}}$ sensor mitoCAR-GECO1. Patient cells showed a greater increase in $[\text{Ca}^{2+}]_{\text{m}}$ at the injury site, which took longer to return to preinjury baseline, resulting in an excessive $[\text{Ca}^{2+}]_{\text{m}}$ load (Fig. 3, K–M). This $[\text{Ca}^{2+}]_{\text{m}}$ overload caused large-scale depolarization of mitochondria, as demonstrated by the mitochondrial potential-sensitive dye tetramethylrhodamine, ethyl ester (TMRE; Fig. 3, N and O; and Fig. S2). In contrast to healthy myoblasts, where PM injury caused the mitochondrial potential to transiently increase before returning to preinjury level within the next minute, mitochondria in patient cells were increasingly depolarized following injury (Fig. 3 O). These results show that ER Ca^{2+} imbalance in ANO5 patient cells disrupts multiple Ca^{2+} -dependent PMR processes.

ANO5 deficit impairs myofiber PMR, which is addressed by ameliorating $[\text{Ca}^{2+}]_{\text{c}}$ overload

ANO5 is preferentially expressed in muscles (Fig. S3), and its deficit causes muscular dystrophy. To test whether the above

findings in patient myoblasts extend to mature muscle fibers, we generated ANO5-KO mouse by deleting exons 10–12 from the ANO5 gene. Laser injury of isolated flexor digitorum brevis (FDB) myofibers showed that compared with the WT myofibers, ANO5-KO myofibers allowed significantly higher FM1-43 dye entry, and nearly twice as many ANO5-KO myofibers failed to repair compared with WT myofibers (Fig. 4, A–C). To test the myofiber repair ability, we also examined this in an independent muscle, the extensor digitorum longus (EDL). Myofibers in intact EDL muscles isolated from 10-mo-old ANO5-KO mice also repaired poorly following laser injury, as indicated by greater FM1-43 dye entry into the myofiber (Fig. 4, D and E). To further confirm the poor repair ability of ANO5-deficient myofibers, we monitored their ability to recover from eccentric exercise-induced myofiber injury. Isolated EDL muscles from these animals showed that force loss following 10% lengthening contraction (LC) injury was significantly greater for EDL muscles from ANO5-KO mice compared with the age-matched WT mice (Fig. 4 F). Greater LC-induced damage could be due to sarcoplasmic reticulum Ca^{2+} imbalance during excitation-contraction coupling. However, neither the level of the sarcoplasmic reticulum Ca^{2+} release channel RYR1 nor Ca^{2+} homeostasis during myofiber contraction showed any dysregulation in ANO5-KO mice (Fig. S3). Together, the findings above indicate that the force loss following LC contraction was due to poor repair of damaged myofibers. This was confirmed by the enhanced entry of membrane-impermeant dye (procion orange [PO]) in EDL myofibers from LC-injured ANO5-KO muscle as compared with WT muscle (Fig. 4, G and H).

The findings above show that excess $[\text{Ca}^{2+}]_{\text{c}}$ is the cellular deficit that leads to poor PMR of ANO5-deficient muscle cells. Muscle diseases associated with $[\text{Ca}^{2+}]_{\text{c}}$ overload benefit from SERCA1 overexpression (Goonasekera et al., 2011; Mázala et al., 2015). To assess the potential for such a therapeutic approach, we first examined SERCA1 protein expression. Compared with WT mice, muscles in ANO5-KO mice express higher levels of SERCA1 (Fig. 4, I and J). Thus, as an alternate to SERCA overexpression, we hypothesized that pharmacologically sequestering the acute increase in $[\text{Ca}^{2+}]_{\text{c}}$ may improve the repair ability of ANO5-deficient muscle fibers. As a proof of principle for this therapeutic approach, we employed a potent Ca^{2+} chelator, 1,2-bis(o-aminophenoxy)ethane- N,N,N',N' -tetraacetic acid (BAPTA), that can be loaded into live cells in its acetoxymethyl ester form (BAPTA-AM). Acute (20-min) treatment of ANO5-KO myofibers with BAPTA-AM efficiently reduced injury-triggered increase in $[\text{Ca}^{2+}]_{\text{c}}$ to levels comparable to WT myofibers (Fig. 4, K and L). BAPTA-AM treatment did not perturb the peak $[\text{Ca}^{2+}]_{\text{c}}$ increase following PM injury (Fig. 4 M) but instead worked by reducing the time taken for the increase in $[\text{Ca}^{2+}]_{\text{c}}$ to return to baseline, allowing the overall injury-triggered $[\text{Ca}^{2+}]_{\text{c}}$ load to return to WT levels (Fig. 4, N and O). This amelioration of $[\text{Ca}^{2+}]_{\text{c}}$ overload

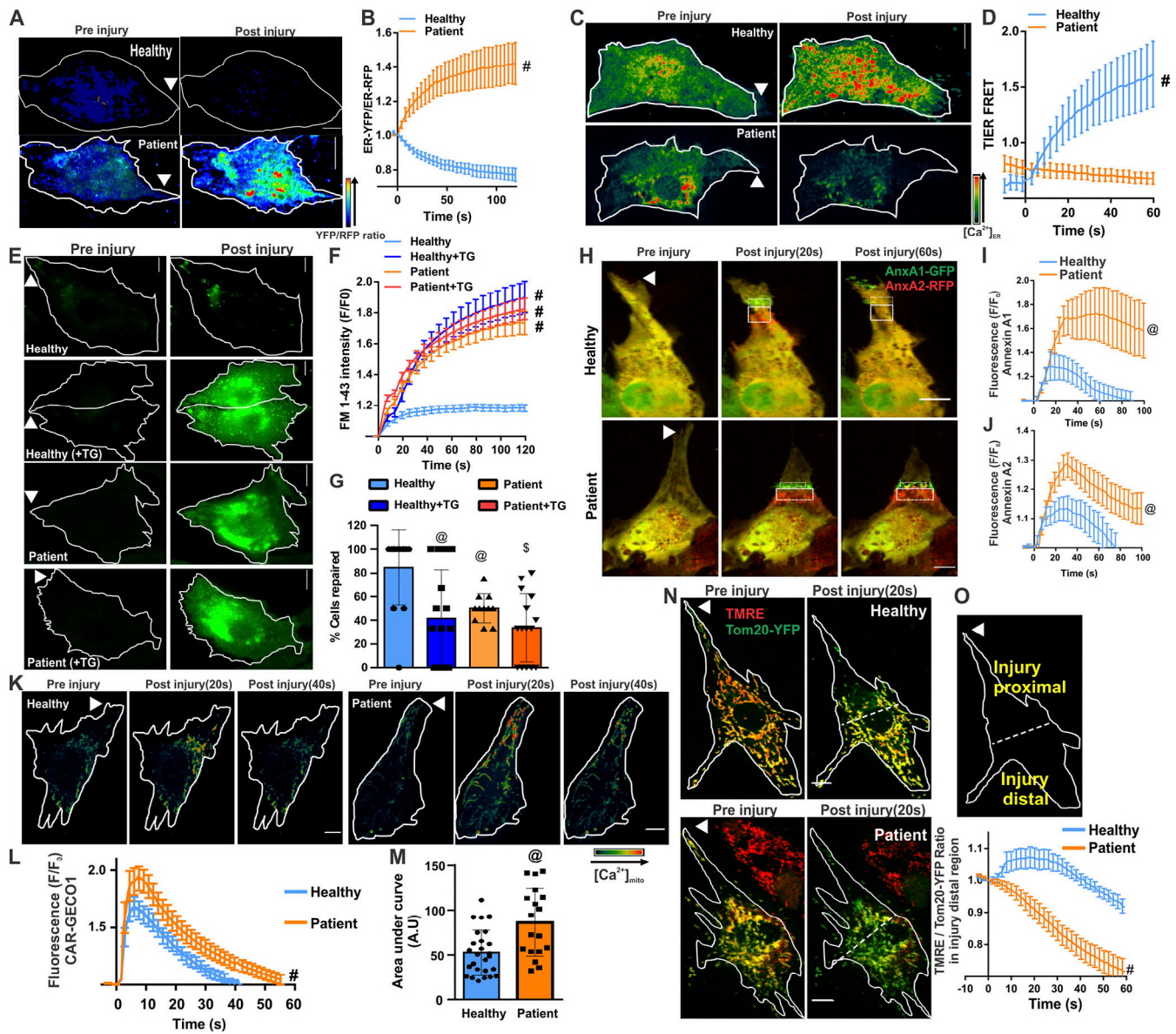


Figure 3. ANO5 is an ER-resident ion channel that regulates $[Ca^{2+}]_c$ during PMR. (A and B) Pseudocolored images (A) and quantification (B) of the kinetics of change in fluorescence of Cl^- -sensitive YFP and Cl^- -insensitive RFP fluorescence targeted to ER in healthy and ANO5-deficient patient myoblasts. $n = 18$ (healthy control) and 15 (patient) cells. (C and D) Pseudocolored images (C) and plot (D) showing quantification of T1ER FRET ratios before and 60 s after injury of healthy and patient cells. $n = 20$ (healthy) and 19 (patient) cells. (E and F) Images (E) and plots (F) showing FMI-43 dye entry in healthy and patient cells treated or untreated with the SERCA inhibitor TG. $n = 16$ (healthy), 31 (healthy, TG), 33 (patient), and 45 (patient, TG) cells. (G) Percentage of myoblasts in E and F that repaired following PM injury after indicated treatments. (H) Images before and 60 s after injury. (I and J) Plots showing average kinetics of annexin A1-GFP (AnxA1-GFP; I) and (J) annexin A2-RFP (AnxA2-RFP) accumulation at the repair site (marked by boxes) of healthy and patient myoblasts coexpressing annexin A1-GFP and annexin A2-RFP. $n = 22$ (healthy) and 18 (patient) cells. (K) Pseudocolored images of healthy and patient myoblasts expressing the mitochondrial calcium sensor CAR-GECO1 imaged during the course of PMR. (L and M) Plots showing quantification of normalized CAR-GECO1 fluorescence in healthy and patient myoblasts during PMR. $n = 26$ (healthy) and 18 cells (patient). A.U., arbitrary units. (N and O) Healthy and patient myoblasts were colabeled using Tom20-YFP (green) and the mitochondrial potential-sensitive dye TMRE (red). (N) Images of cells before and 20 s after injury. (O) Schematic and plot for quantification of the TMRE/YFP ratio in mitochondria in the injury-distal region of the cell (indicated by dotted line). $n = 7$ (healthy) and 15 (patient). Scale bars, 10 μm . Plots show mean \pm SD; @, $P < 0.05$; \$, $P < 0.001$; #, $P < 0.0001$ by Mann-Whitney test or unpaired t test with Welch's correction. Arrowheads indicate site of injury.

significantly improved ANO5-KO myofiber PMR, as shown by reduced FM dye entry and reduction in the number of myofibers that fail to repair to the same level as in WT muscles (Fig. 4, A-C and P-R). These findings show that lack of ANO5 compromises myofiber PMR due to poor $[Ca^{2+}]_c$ buffering following myofiber injury, addressing which could be a therapeutic approach for LGMD2L.

Discussion

Our effort to understand how cells repair from injury has uncovered a novel role of ER in facilitating the PMR in injured cells. PM injury causes a rapid increase in $[Ca^{2+}]_c$, which is efficiently cleared during successful PMR. We find that ER provides the site for the uptake of the injury-triggered cytosolic Ca^{2+} increase. Pharmacologically blocking the activity of the ER calcium pump

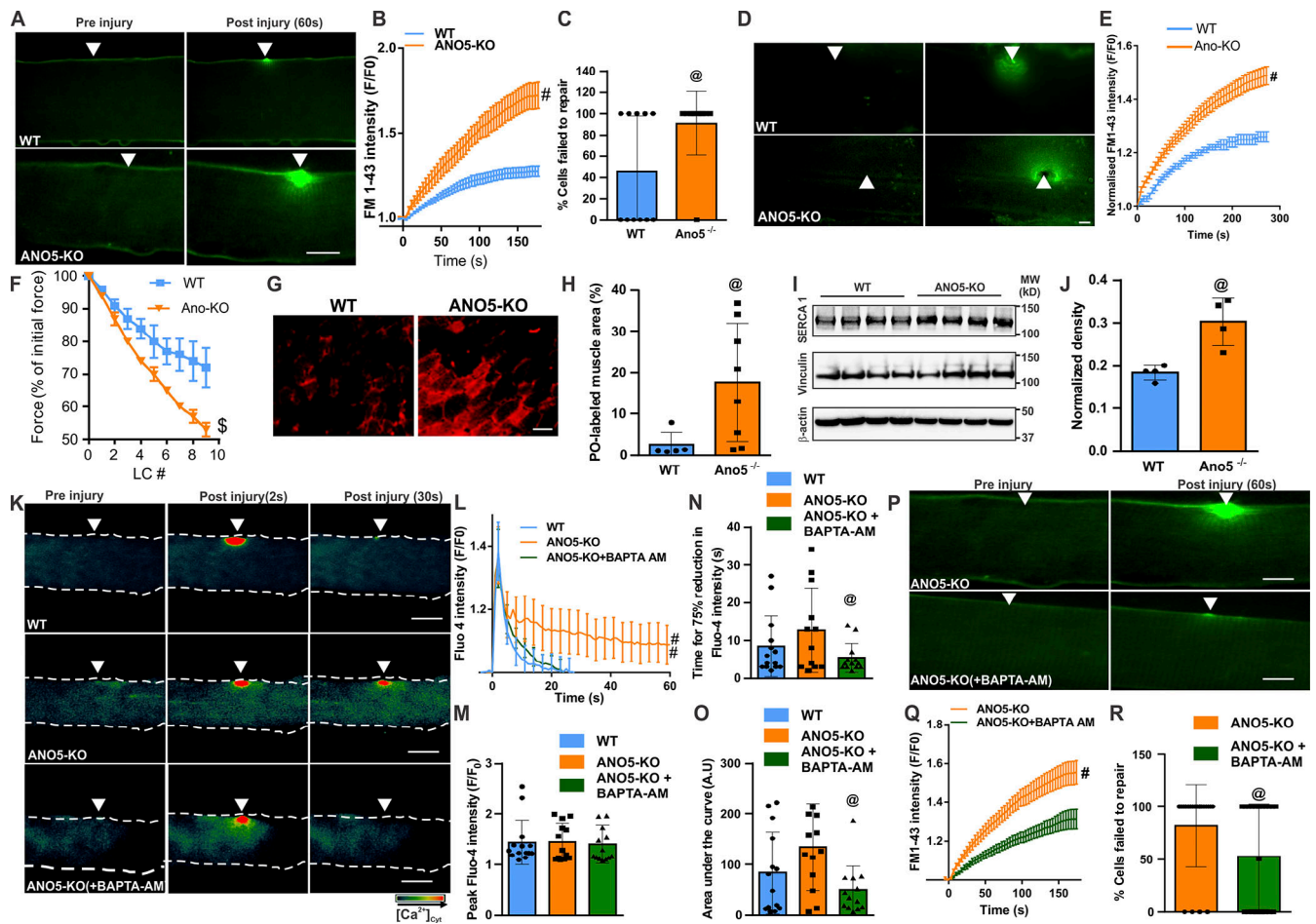


Figure 4. ANO5-KO impairs myofiber repair and is improved by preventing $[Ca^{2+}]_c$ overload. (A–E) Images (A and D) and plots (B and E) showing entry of FM1-43 dye in isolated FDB myofibers (A–C) or intact EDL muscles (D and E) of 10-mo-old ANO5-KO and parental WT mice focally injured by a 10-ms laser pulse. **(C)** Fraction of injured myofibers that failed to repair. $n = 11$ FDB myofibers in each group. $n = 17$ (WT), 19 (KO) EDL myofibers. Arrowheads point to the site of laser injury. **(F)** EDL muscles from 10-mo-old WT and ANO5-KO mice were subjected to mechanical injury by a series of LC injuries. After each round of injury, the muscle contractile force at isometric tetanic stimulation was measured. $n \leq 7$ animals in each group. **(G)** Images showing cross sections of the EDL muscles following eccentric injury, marking myofibers labeled with the cell-impermeant PO dye following LC injury. Scale bar, 50 μm . **(H)** Plot showing quantification of PO labeling. **(I)** Western blots showing SERCA1 levels in bicep muscles from 10-mo-old WT and ANO5-KO mice. **(J)** Plot showing quantification of SERCA1 expression normalized to Vinculin. $n = 4$ mice in each group. **(K)** Pseudocolored images of Fluo-4-labeled isolated FDB myofibers of WT or ANO5-KO mice injured before or following incubation in the cytoplasmic Ca^{2+} chelator BAPTA-AM (10 μM). **(L)** Plots showing kinetics of change in Fluo-4 fluorescence. **(M)** Plot showing peak Fluo-4 fluorescence. **(N)** Time for the peak Fluo-4 fluorescence to reduce by 75%. **(O)** Area under the Fluo-4 kinetics plot for the various groups of myofibers injured. $n = 14$ (WT, DMSO), 13 (ANO5-KO, DMSO), 13 (ANO5-KO + BAPTA-AM). **(P and Q)** Images (P) and plot (Q) showing FM1-43 dye entry into isolated FDB myofibers from ANO5-KO mice following treatment with DMSO or BAPTA-AM. **(R)** Quantification of the fraction of injured myofibers that failed to repair. $n = 11$ myofibers in each group. Scale bars for A, D, K, and P, 10 μm . Plots in B, E, L, and Q show mean \pm SEM. Rest of the plots show mean \pm SD. @, $P < 0.05$; \$, $P < 0.001$; #, $P < 0.0001$, Mann-Whitney or unpaired t test with Welch’s correction.

by TG leads to $[Ca^{2+}]_c$ overload in the injured cells and results in poor repair. We also identify that ER-mediated clearance of the $[Ca^{2+}]_c$ in the injured cells requires the CaCC ANO5. Upon being activated by the injury-triggered increase in $[Ca^{2+}]_c$, ANO5 enables the transport of anion into the ER. The anions pumped into the ER then serve as the counter ion for facilitating sequestration of Ca^{2+} pumped into the ER by SERCA activity. Such a role has been shown for the ER-localized CaCC protein bestrophin 1 in retinal pigment epithelial cells (Neusser et al., 2010). Here, we show an analogous role of ANO5 in muscle cells, which is consistent with its localization at the ER (Chandra et al., 2019; Tsutsumi et al., 2005; Tsutsumi et al., 2004). This role of ANO5 in PMR is supported by our studies using the CaCC inhibitor

NPPB, which causes injury-triggered Ca^{2+} overload and poor PMR phenotype, in healthy cells. Together, the above findings show that during PMR, SERCA and CaCC both work in concert to enable Ca^{2+} -activated $[Ca^{2+}]_c$ clearance by the ER. Blocking either of these transporters in healthy cells causes $[Ca^{2+}]_c$ overload upon PM injury and compromises PMR.

Using ANO5-deficient patient myoblasts and fibroblasts as models for genetic deficit of ER-resident CaCC, we find that failure of ER calcium uptake in these cells disturbs annexin reparative response following injury and causes $[Ca^{2+}]_m$ overload. Together, these deficits lead to excessive mitochondrial depolarization and dysfunction. Disruption of these repair process leads to poor PMR due to the failure of ER to uptake calcium.

Further, using the ANO5-KO mouse model, we establish that the role of ANO5 in membrane repair is conserved in skeletal myofibers. These results support the findings in an unrelated ANO5-KO mouse model, where a myofiber sarcolemmal repair deficit was observed (Griffin et al., 2016). While mitochondrial abnormalities were reported in this ANO5-KO mouse model (Griffin et al., 2016), how ANO5 deficiency causes this defect was not resolved. We find that reduction in mitochondrial number and function in myofibers of *mdx* mice (an animal model of Duchenne muscular dystrophy) results in poor PMR (Vila et al., 2017). In ANO5-deficient cells, cytosolic Ca^{2+} overload leads to excessive mitochondrial Ca^{2+} accumulation, resulting in loss of mitochondrial membrane potential in injured cells, which affects multiple calcium-dependent PMR processes. Key among them is the mitochondria, which, in injured ANO5 patient cells, gets overloaded with Ca^{2+} and loses membrane potential. Mitochondrial depolarization and dysregulated calcium homeostasis lead to altered mitochondrial redox signaling required for actin-mediated PM wound closure and this mitochondria-mediated PMR response is compromised in several diseases (Boehler et al., 2019; Debattisti et al., 2019; Horn et al., 2020). As mitochondrial pathology in ANO5-deficient cells is downstream of primary deficit in ER calcium handling by the injured cells, it raises the possibility that addressing mitochondrial deficit may offer therapeutic benefits.

Calcium influx triggered by the PM injury is a widely recognized prerequisite for the activation of PMR. However, our study highlights the Goldilocks-like nature of calcium during PMR, such that an increase in $[Ca^{2+}]_c$ that is either too little or too much increase is detrimental to PMR. We previously observed that excessive $[Ca^{2+}]_c$ increase affects ER (Chandra et al., 2019) and here we find that this also dysregulates the annexin-dependent vesicle-mediated PMR and cytoskeleton-mediated PM wound closure through mitochondrial signaling. Thus, just as a lack of Ca^{2+} increase, extended and excessive Ca^{2+} increase following PM injury impairs PMR. Ca^{2+} excess does so by protracted and excessive response by Annexins and mitochondria, which represent the PMR machineries involved in membrane and cytoskeletal remodeling. These findings also help explain the reports of mitochondrial abnormalities (Griffin et al., 2016), and aberrant annexin response (Foltz et al., 2020 Preprint) in skeletal muscles in another ANO5-KO mouse model.

Similar to the ANO5 deficit in LGMD2L, poor sarcolemmal repair is also a feature of LGMD2B, which is caused by a lack of the muscle protein dysferlin (Bansal et al., 2003; Bashir et al., 1998). However, unlike dysferlin-deficient muscle cells, where the PMR deficit is caused by poor lysosomal exocytosis (Defour et al., 2014b), ANO5-deficient cells show normal injury-triggered lysosomal exocytosis (Jaiswal et al., 2007). Thus, the cellular basis of poor PMR in ANO5-deficient cells appears to be distinct from the poor repair of dysferlin-deficient cells. This is supported by the failure of increased ANO5 expression to rescue muscle pathology in dysferlin-deficient mice (Monjaret et al., 2013). In this study, we show that the functional role of ANO5 in muscle cell is to facilitate Ca^{2+} homeostasis during PMR. This role of ANO5 is supported by our findings that reversing the $[Ca^{2+}]_c$ overload in ANO5-deficient injured skeletal myofibers

improves their repair. It also provides a potential pharmacological strategy for addressing the cellular deficit in muscular dystrophy caused by the ANO5 deficit.

In summary, our study adds ER to the list of organelles that are required for efficient PMR and identifies the basis for poor PMR in ANO5-deficient muscles. It describes the mechanism for calcium-activated ER calcium homeostasis and makes use of patient cells and a mouse model to establish that calcium dysregulation leading to dysfunction in mitochondrial and annexin-mediated repair responses leads to poor PMR (Boehler et al., 2019; Debattisti et al., 2019; Horn et al., 2020; Horn et al., 2017; Vila et al., 2017). Lack of ANO5 causes excessive mitochondrial Ca^{2+} overload and loss of membrane potential, leading to PMR deficit. Our findings identify the requirement of the ER in PMR and show that a deficit in this process contributes to disease, uncovering a new aspect of the ER in maintaining healthy cell physiology and cell survival.

Materials and methods

Cells and treatments

LGMD2L fibroblasts were used as described previously (Jaiswal et al., 2007). Myoblasts were generated as described previously (Chandra et al., 2019) and were cultured in Skeletal Muscle Cell Basal Media (PromoCell) containing 15% FBS, 5% fetal calf serum, and all the necessary supplements (human EGF, basic FGF from human, fetuin, insulin, and dexamethasone) as described previously (Chandra et al., 2019). Transfections were performed in OPTI-MEM (Invitrogen) using Lipofectamine LTX for 4 h followed by addition of full growth media and growing the cells for 24–48 h.

Animals

WT mice (C57BL/6) were obtained from Jackson Laboratory. Methods involving animals were approved by the institutional animal care and use committee. All the animal procedures were performed in accordance with the approved guidelines. Animals were maintained in a facility accredited by the American Association for Accreditation of Laboratory Animal Care. 10-month-old male and female animals were used for all experimental procedures. Construction of the targeting vector for ANO5-KO mice and generation of these mice was performed at the Genoway. The positive embryonic stem cell (ES) clones were injected into C57BL/6J blastocysts that were reimplanted into foster mothers to generate chimeric mice. Germline transmission was obtained through the breeding of male chimeras with females transgenic for cytomegalovirus-Cre recombinase, which permits the excision of the neo cassette. The Cre transgene was segregated by a first cross on C57BL/6 background; the resulting heterozygous mice were backcrossed for 10 generations on the C57BL/6 (mice were from Charles River) and then interbred. For genotyping, genomic DNA from mouse tail was extracted and amplified using KAPA2G Fast HotStart Genotyping PCR Kit (KK5621; KAPA Biosystems), with the following primers chosen in the ANO5 gene: Flp.F, 5'-TCTTCATGGGGATCTGGGGTGTAGT A-3', Flp.R, 5'-CCCTAGAACTACATAATCTTGGTGTGGTGTAG-3', and 49683cre.F, 5'-ATTCTGAGAATATGTGTAATTGTGGC

AGC-3'. The resulting WT and mutant alleles generated PCR fragments of 318 and 890 bp, respectively.

Ca²⁺ and Cl⁻ measurement assays

For measuring the [Ca²⁺]_c, myoblasts and fibroblasts cultured on coverslips were incubated with DMEM without FBS containing 10 μM Fluo-4-AM (Life Technologies) for 20 min at 37°C and 5% CO₂. After washing with prewarmed cell imaging medium (CIM), cells were laser injured as described before (Defour et al., 2014a). To monitor Ca²⁺ influx, injured cells were imaged at an interval of four to six frames/second for the 3 min after injury using IX81 microscope (Olympus America) custom equipped with a CSUX1 spinning disc confocal unit (Yokogawa Electric). Images were collected using a 60× oil-immersion objective (1.45 NA). Images were acquired using an Evolve 512 high-performance electron multiplying charge-coupled device (EMCCD) camera (Teledyne Photometrics) at 1 Hz. Image acquisition and laser injury was controlled using Slidebook 6.0 (Intelligent Imaging Innovations). For every image, the kinetics of Ca²⁺ influx was expressed by measuring the cellular Fluo-4-AM emission, which responds to the free cytosolic Ca²⁺. For measuring the free Ca²⁺ in the ER, we used FRET-based biosensor, T1ER (Abell et al., 2011). Myoblasts were transfected with T1ER plasmid DNA 24 h before the cells were injured (in presence of 2 mM Ca²⁺). Pseudocolored images representing fluorescence intensity were generated using Slidebook 6.0. For measuring the mitochondrial Ca²⁺, we used the mitochondrial Ca²⁺ sensor CAR-GECO1 as described previously (Wu et al., 2013). To monitor ER Cl⁻ levels, cells were transfected with KDEL-YFP and KDEL-RFP plasmids 24 h before the assay. Calcium-activated chloride influx into the ER was measured for 2 min following PM injury by measuring the ratio of YFP and RFP fluorescence (Jayaraman et al., 2000; Kuner and Augustine, 2000).

Laser injury assays

Cells cultured on coverslips were transferred to and incubated in CIM/PBS buffer with 1 mg/ml FM1-43 dye (Life Technologies) and placed in a Tokai Hit microscopy stage-top ZILCS incubator (Tokai Hit) maintained at 37°C. For laser injury, a 1- to 5-μm² area was irradiated for 10 ms with a pulsed laser (Ablate!; 3i Intelligent Imaging Innovations). Cells were imaged using IX81 microscope (Olympus America). The change in FM dye intensity ($\Delta F/F$ where F is the intensity at the start of imaging) was used to quantify cell membrane repair kinetics. Images were acquired at 2-s intervals, and data shown in the plots represent frames that are 10 s apart. For myofiber injury, muscles were surgically isolated from euthanized WT or ANO5-KO mice in Tyrode's solution, and laser injury was performed using the microscope and laser injury settings as described previously (Defour et al., 2014a; Leikina et al., 2015) in the Tyrode's buffer containing 1.33 mg/ml FM1-43 dye. For isolating FDB myofibers, we used a method previously described (Mázala et al., 2015). Briefly, FDB muscles were dissected from deeply anaesthetized animals, and single muscle fibers were obtained by collagenase digestion with type 2 collagenase (Worthington) in minimal essential medium with 10% FBS and 1% penicillin-streptomycin (Invitrogen). After

incubation at 37°C in a CO₂ incubator (95% O₂/5% CO₂), single muscle fibers were obtained by trituration with fire-polished glass pipettes. FDB fibers were maintained in minimal essential medium with 10% FBS at 37°C, 95% O₂/5% CO₂ overnight and used for experiment in the next day. The kinetics of repair was determined by measuring the cellular FM1-43 fluorescence. FM1-43 intensity (F/F_0 , where F₀ is the original value at time 0) was used to quantify the kinetics of cell membrane repair.

Western blotting

Cells were lysed with RIPA buffer (Sigma-Aldrich) containing protease inhibitor cocktail (Thermo Fisher Scientific). Proteins transferred to nitrocellulose membranes were probed with the indicated antibodies against SERCA1, vinculin, RyR1, and β-actin (all from Santa Cruz Biotechnology). Primary antibodies were followed by the appropriate HRP-conjugated secondary antibodies (Sigma-Aldrich) and chemiluminescent Western blotting substrate (Thermo Fisher Scientific; GE Healthcare). The blots were then processed on the Bio-Rad ChemiDoc Touch Imaging System.

Measurement of mitochondrial membrane potential

Myoblasts were incubated with the potentiometric dye TMRE for 15 min at 37°C and washed three times in CIM, and then we performed laser injury. These cells were previously transfected with Tom20-GFP, and the ratio of fluorescence intensities at 561 nm and 488 nm was considered as an index of mitochondrial membrane potential.

Contraction-induced myofiber sarcolemmal injury

After anesthetizing the mice with a mixture of ketamine and xylazine, EDL muscles from the right hindlimb of C57BL/6 and ANO5-KO mice were carefully exposed, and 6–0 silk sutures were firmly attached to proximal and distal tendons. The EDL was dissected and placed in a bath containing buffered mammalian Ringer's solution (137 mM NaCl, 24 mM NaHCO₃, 11 mM glucose, 5 mM KCl, 2 mM CaCl₂, 1 mM MgSO₄, 1 mM NaH₂PO₄, and 0.025 mM tubocurarine chloride) at 25°C and bubbled with 95% O₂/5% CO₂ to stabilize the pH at 7.4. In the bath, the distal tendon was securely connected to a fixed bottom plate, and the proximal tendon was attached to the arm of a servomotor (800A in vitro muscle apparatus; Aurora Scientific). The vertically aligned EDL muscle was flanked by two stainless steel plate electrodes. Using single 0.2-mm square simulation pulses, the muscle was adjusted to the optimal muscle length (L_0) for force generation. At optimal length, with isometric tetanic contractions 300 ms in duration at frequencies up to 250 Hz separated by 2 min of rest intervals, the maximal force was determined. Specific force, defined as maximal force normalized for the muscle cross-sectional area, was calculated as the maximal force/(muscle mass × (density of muscle tissue × fiber length)⁻¹). The fiber length was based on the fiber to muscle length ratio of 0.45. The muscle tissue density is 1.056 kg/liter. To study contraction-induced sarcolemmal injury, EDL muscles were subjected to nine LCs with 10% strain at a velocity of two fiber lengths per second. Each contraction was separated by a 1-min rest interval. LC-induced force deficits were expressed as

percentage of first contraction. The values were represented as mean \pm SD.

PO and muscle fiber membrane damage

PM injury following LC-induced injury was assessed as before (Vila et al., 2017) using PO dye, which is excluded from myofibers with intact sarcolemma. Immediately after the LC assay, muscles were trimmed of tendons, blotted, weighed, and then incubated while held at L_o in a 0.2% PO solution at room temperature for 30 min, washed in Ringer solution, and quickly frozen in isopentane prechilled with liquid nitrogen. Frozen cross sections of 10- μ m thickness were cut, mounted with fluorescent mounting medium (DAKO), and viewed under a fluorescent microscope to identify the presence of PO. Fields, containing the majority of the muscle cross sections were photographed and scaled under identical conditions at $\times 10$ magnification using Olympus BX61 widefield microscope. By thresholding for unstained muscle, we identified fibers that showed no uptake of PO from fibers that showed PO uptake. From each muscle cross section, the area occupied by PO-labeled fibers ranging from minimal to maximal dye uptake was measured and expressed as a percentage of the complete muscle section area. PO-labeled fibers at the edges of the sections were considered as artifact and were excluded from analysis.

Statistical analysis

For membrane repair analysis, the data are presented as average values for all myoblasts or myofibers used for that analysis. These average values were compared with each other using an unpaired *t* test with Welch's correction performed using Graph Pad Prism software. When the data were not normally distributed or failed the equal variance test, the Mann-Whitney rank sum test was used.

Online supplemental material

Fig. S1 shows that ANO5 deficit reduces ER calcium uptake following purinergic stimulation. Fig. S2 shows monochrome images of data presented in the main figures. Fig. S3 shows ANO5 expression and the effect of its deficit on the ER Ca^{2+} -handling machinery.

Acknowledgments

We thank Dr. Ibrahim Mahjneh (University of Oulu, Oulu, Finland) and Dr. Vincent Mouly (Sorbonne Universit s, Paris, France) for the patient cell line, Tobias Meyer (Stanford Medicine, Stanford, CA) for the gift of pcDNA-T1ER (plasmid 47928; Addgene), and Robert Campbell (University of Alberta, Edmonton, Alberta, Canada) for the gift of cytomegalovirus-mitochondria-GECO1 (plasmid 46022; Addgene). We thank Dr. Anamaris Colberg-Poley and members of our laboratory for helpful comments during the course of this work.

I. Richard acknowledges financial support from Association Fran aise contre les Myopathies. J.K. Jaiswal acknowledges financial support from the National Institute of Arthritis and Musculoskeletal and Skin Diseases (grant R01AR055686) and

the National Institute of Child Health and Human Development (grant U54HD090257).

The authors declare no competing financial interests. Author contributions: G. Chandra and J.K. Jaiswal designed the study. G. Chandra performed experiments through help from S.C. Sreetama with cellular studies, D. M zala with myofiber calcium measurements, and J.H. VanderMeulen with muscle physiology studies. I. Richard and K. Charton generated and genetically characterized the KO mouse model. J.K. Jaiswal conceived the study, acquired funding, helped with data analysis, and wrote the manuscript together with G. Chandra, and with help from all authors.

Submitted: 6 June 2020

Revised: 11 December 2020

Accepted: 27 January 2021

References

- Abell, E., R. Ahrends, S. Bandara, B.O. Park, and M.N. Teruel. 2011. Parallel adaptive feedback enhances reliability of the Ca^{2+} signaling system. *Proc. Natl. Acad. Sci. USA*. 108:14485-14490. <https://doi.org/10.1073/pnas.1018266108>
- Bansal, D., K. Miyake, S.S. Vogel, S. Groh, C.C. Chen, R. Williamson, P.L. McNeil, and K.P. Campbell. 2003. Defective membrane repair in dysferlin-deficient muscular dystrophy. *Nature*. 423:168-172. <https://doi.org/10.1038/nature01573>
- Bashir, R., S. Britton, T. Strachan, S. Keers, E. Vafiadaki, M. Lako, I. Richard, S. Marchand, N. Bourg, Z. Argov, et al. 1998. A gene related to Caenorhabditis elegans spermatogenesis factor fer-1 is mutated in limb-girdle muscular dystrophy type 2B. *Nat. Genet.* 20:37-42. <https://doi.org/10.1038/1689>
- Berg, J., H. Yang, and L.Y. Jan. 2012. Ca^{2+} -activated Cl⁻ channels at a glance. *J. Cell Sci.* 125:1367-1371. <https://doi.org/10.1242/jcs.093260>
- Bittel, A.J., S.C. Sreetama, D.C. Bittel, A. Horn, J.S. Novak, T. Yokota, A. Zhang, R. Maruyama, K. Rowel Q Lim, J.K. Jaiswal, and Y.-W. Chen. 2020. Membrane Repair Deficit in Facioscapulohumeral Muscular Dystrophy. *Int. J. Mol. Sci.* 21:5575. <https://doi.org/10.3390/ijms21155575>
- Boehler, J.F., A. Horn, J.S. Novak, N. Li, S. Ghimbovski, I.E. Lundberg, H. Alexanderson, L. Alemo Munters, J.K. Jaiswal, and K. Nagaraju. 2019. Mitochondrial dysfunction and role of harakiri in the pathogenesis of myositis. *J. Pathol.* 249:215-226. <https://doi.org/10.1002/path.5309>
- Bolduc, V., G. Marlow, K.M. Boycott, K. Saleki, H. Inoue, J. Kroon, M. Itakura, Y. Robitaille, L. Parent, F. Baas, et al. 2010. Recessive mutations in the putative calcium-activated chloride channel Anoctamin 5 cause proximal LGMD2L and distal MMD3 muscular dystrophies. *Am. J. Hum. Genet.* 86:213-221. <https://doi.org/10.1016/j.ajhg.2009.12.013>
- Chandra, G., A. Defour, K. Mamchoui, K. Pandey, S. Mishra, V. Mouly, S. Sreetama, M. Mahad Ahmad, I. Mahjneh, H. Morizono, et al. 2019. Dysregulated calcium homeostasis prevents plasma membrane repair in Anoctamin 5/TMEM16E-deficient patient muscle cells. *Cell Death Discov.* 5:118. <https://doi.org/10.1038/s41420-019-0197-z>
- Chen, J., A. Sitsel, V. Benoy, M.R. Sep lveda, and P. Vangheluwe. 2020. Primary Active Ca^{2+} Transport Systems in Health and Disease. *Cold Spring Harb. Perspect. Biol.* 12:a035113. <https://doi.org/10.1101/cshperspect.a035113>
- Cooper, S.T., and P.L. McNeil. 2015. Membrane Repair: Mechanisms and Pathophysiology. *Physiol. Rev.* 95:1205-1240. <https://doi.org/10.1152/physrev.00037.2014>
- Debattisti, V., A. Horn, R. Singh, E.L. Seifert, M.W. Hogarth, D.A. Mazala, K.T. Huang, R. Horvath, J.K. Jaiswal, and G. Hajn czi. 2019. Dysregulation of Mitochondrial Ca^{2+} Uptake and Sarcolemma Repair Underlie Muscle Weakness and Wasting in Patients and Mice Lacking MICU1. *Cell Rep.* 29:1274-1286.e6. <https://doi.org/10.1016/j.celrep.2019.09.063>
- Defour, A., S.C. Sreetama, and J.K. Jaiswal. 2014a. Imaging cell membrane injury and subcellular processes involved in repair. *J. Vis. Exp.* (85). <https://doi.org/10.3791/51106>
- Defour, A., J.H. Van der Meulen, R. Bhat, A. Bigot, R. Bashir, K. Nagaraju, and J.K. Jaiswal. 2014b. Dysferlin regulates cell membrane repair by

- facilitating injury-triggered acid sphingomyelinase secretion. *Cell Death Dis.* 5:e1306. <https://doi.org/10.1038/cddis.2014.272>
- Demonbreun, A.R., M. Quattrocchi, D.Y. Barefield, M.V. Allen, K.E. Swanson, and E.M. McNally. 2016. An actin-dependent annexin complex mediates plasma membrane repair in muscle. *J. Cell Biol.* 213:705–718. <https://doi.org/10.1083/jcb.201512022>
- Di Zanni, E., A. Gradogna, J. Scholz-Starke, and A. Boccaccio. 2018. Gain of function of TMEM16E/ANO5 scrambling activity caused by a mutation associated with gnathodiaphyseal dysplasia. *Cell. Mol. Life Sci.* 75: 1657–1670. <https://doi.org/10.1007/s00018-017-2704-9>
- Di Zanni, E., A. Gradogna, C. Picco, J. Scholz-Starke, and A. Boccaccio. 2020. TMEM16E/ANO5 mutations related to bone dysplasia or muscular dystrophy cause opposite effects on lipid scrambling. *Hum. Mutat.* 41: 1157–1170. <https://doi.org/10.1002/humu.24006>
- Dreinhöfer, J., H. Gögelein, and R. Greger. 1988. Blocking kinetics of Cl⁻ channels in colonic carcinoma cells (HT29) as revealed by 5-nitro-2-(3-phenylpropylamino)benzoic acid (NPPB). *Biochim. Biophys. Acta.* 946: 135–142. [https://doi.org/10.1016/0005-2736\(88\)90466-X](https://doi.org/10.1016/0005-2736(88)90466-X)
- Duran, C., Z. Qu, A.O. Osunkoya, Y. Cui, and H.C. Hartzell. 2012. ANOs 3–7 in the anoctamin/Tmem16 Cl⁻ channel family are intracellular proteins. *Am. J. Physiol. Cell Physiol.* 302:C482–C493. <https://doi.org/10.1152/ajpcell.00140.2011>
- Foltz, S.J., Y. Cui, H.J. Choo, and H.C. Hartzell. 2020. Defective Trafficking of Annexins to the Site of Injury in ANO5-Knockout Muscle Fibers. *bioRxiv.* 10.1101/2020.05.22.110825 (Preprint posted May 24, 2020)
- Goonasekera, S.A., C.K. Lam, D.P. Millay, M.A. Sargent, R.J. Hajjar, E.G. Kranias, and J.D. Molkentin. 2011. Mitigation of muscular dystrophy in mice by SERCA overexpression in skeletal muscle. *J. Clin. Invest.* 121: 1044–1052. <https://doi.org/10.1172/JCI43844>
- Griffin, D.A., R.W. Johnson, J.M. Whitlock, E.R. Pozsgai, K.N. Heller, W.E. Grose, W.D. Arnold, Z. Sahenk, H.C. Hartzell, and L.R. Rodino-Klapac. 2016. Defective membrane fusion and repair in Anoctamin5-deficient muscular dystrophy. *Hum. Mol. Genet.* 25:1900–1911. <https://doi.org/10.1093/hmg/ddw063>
- Han, R., M. Kanagawa, T. Yoshida-Moriguchi, E.P. Rader, R.A. Ng, D.E. Michele, D.E. Muirhead, S. Kunz, S.A. Moore, S.T. Iannaccone, et al. 2009. Basal lamina strengthens cell membrane integrity via the laminin G domain-binding motif of alpha-dystroglycan. *Proc. Natl. Acad. Sci. USA.* 106:12573–12579. <https://doi.org/10.1073/pnas.0906545106>
- Hicks, D., A. Sarkozy, N. Muelas, K. Köehler, A. Huebner, G. Hudson, P.F. Chinnery, R. Barresi, M. Eagle, T. Polvikoski, et al. 2011. A founder mutation in Anoctamin 5 is a major cause of limb-girdle muscular dystrophy. *Brain.* 134:171–182. <https://doi.org/10.1093/brain/awq294>
- Horn, A., and J.K. Jaiswal. 2018. Cellular mechanisms and signals that coordinate plasma membrane repair. *Cell. Mol. Life Sci.* 75:3751–3770. <https://doi.org/10.1007/s00018-018-2888-7>
- Horn, A., J.H. Van der Meulen, A. Defour, M. Hogarth, S.C. Sreetama, A. Reed, L. Scheffer, N.S. Chandel, and J.K. Jaiswal. 2017. Mitochondrial redox signaling enables repair of injured skeletal muscle cells. *Sci. Signal.* 10: eaaj1978.
- Horn, A., S. Raavicharla, S. Shah, D. Cox, and J.K. Jaiswal. 2020. Mitochondrial fragmentation enables localized signaling required for cell repair. *J. Cell Biol.* 219:e201909154. <https://doi.org/10.1083/jcb.201909154>
- Huang, F., X. Wong, and L.Y. Jan. 2012. International Union of Basic and Clinical Pharmacology. LXXXV: calcium-activated chloride channels. *Pharmacol. Rev.* 64:1–15. <https://doi.org/10.1124/pr.111.005009>
- Jaiswal, J.K. 2001. Calcium - how and why? *J. Biosci.* 26:357–363. <https://doi.org/10.1007/BF02703745>
- Jaiswal, J.K., and J. Nylandsted. 2015. S100 and annexin proteins identify cell membrane damage as the Achilles heel of metastatic cancer cells. *Cell Cycle.* 14:502–509. <https://doi.org/10.1080/15384101.2014.995495>
- Jaiswal, J.K., G. Marlow, G. Summerill, I. Mahjneh, S. Mueller, M. Hill, K. Miyake, H. Haase, L.V. Anderson, I. Richard, et al. 2007. Patients with a non-dysferlin Miyoshi myopathy have a novel membrane repair defect. *Traffic.* 8:77–88. <https://doi.org/10.1111/j.1600-0854.2006.00505.x>
- Jaiswal, J.K., S.P. Lauritzen, L. Scheffer, M. Sakaguchi, J. Bunkenborg, S.M. Simon, T. Kallunki, M. Jäättelä, and J. Nylandsted. 2014. S100A11 is required for efficient plasma membrane repair and survival of invasive cancer cells. *Nat. Commun.* 5:3795. <https://doi.org/10.1038/ncomms4795>
- Jayaraman, S., P. Haggie, R.M. Wachter, S.J. Remington, and A.S. Verkman. 2000. Mechanism and cellular applications of a green fluorescent protein-based halide sensor. *J. Biol. Chem.* 275:6047–6050. <https://doi.org/10.1074/jbc.275.9.6047>
- Kuner, T., and G.J. Augustine. 2000. A genetically encoded ratiometric indicator for chloride: capturing chloride transients in cultured hippocampal neurons. *Neuron.* 27:447–459. [https://doi.org/10.1016/S0896-6273\(00\)00056-8](https://doi.org/10.1016/S0896-6273(00)00056-8)
- Leikina, E., A. Defour, K. Melikov, J.H. Van der Meulen, K. Nagaraju, S. Bhuvanendran, C. Gebert, K. Pfeifer, L.V. Chernomordik, and J.K. Jaiswal. 2015. Annexin A1 Deficiency does not Affect Myofiber Repair but Delays Regeneration of Injured Muscles. *Sci. Rep.* 5:18246. <https://doi.org/10.1038/srep18246>
- Mázala, D.A., S.J.P. Pratt, D. Chen, J.D. Molkentin, R.M. Lovering, and E.R. Chin. 2015. SERCA1 overexpression minimizes skeletal muscle damage in dystrophic mouse models. *Am. J. Physiol. Cell Physiol.* 308:C699–C709. <https://doi.org/10.1152/ajpcell.00341.2014>
- McNeil, P.L., and R.A. Steinhardt. 2003. Plasma membrane disruption: repair, prevention, adaptation. *Annu. Rev. Cell Dev. Biol.* 19:697–731. <https://doi.org/10.1146/annurev.cellbio.19.111301.140101>
- Møller, J.V., C. Olesen, A.M. Winther, and P. Nissen. 2010. The sarcoplasmic Ca²⁺-ATPase: design of a perfect thermo-osmotic pump. *Q. Rev. Biophys.* 43:501–566. <https://doi.org/10.1017/S00338351000017X>
- Monjaret, F., L. Suel-Petat, N. Bourg-Alibert, A. Vihola, S. Marchand, C. Roudaut, E. Gicquel, B. Udd, I. Richard, and K. Charton. 2013. The phenotype of dysferlin-deficient mice is not rescued by adeno-associated virus-mediated transfer of anoctamin 5. *Hum. Gene Ther. Clin. Dev.* 24:65–76. <https://doi.org/10.1089/humc.2012.217>
- Neussert, R., C. Müller, V.M. Milenkovic, and O. Strauss. 2010. The presence of bestrophin-1 modulates the Ca²⁺ recruitment from Ca²⁺ stores in the ER. *Pflugers Arch.* 460:163–175. <https://doi.org/10.1007/s00424-010-0840-2>
- Palmer, A.E., M. Giacomello, T. Kortemme, S.A. Hires, V. Lev-Ram, D. Baker, and R.Y. Tsien. 2006. Ca²⁺ indicators based on computationally redesigned calmodulin-peptide pairs. *Chem. Biol.* 13:521–530. <https://doi.org/10.1016/j.chembiol.2006.03.007>
- Penttilä, S., J. Palmio, T. Suominen, O. Raheem, A. Evilä, N. Muelas Gomez, G. Tasca, L.B. Waddell, N.F. Clarke, A. Barboi, et al. 2012. Eight new mutations and the expanding phenotype variability in muscular dystrophy caused by ANO5. *Neurology.* 78:897–903. <https://doi.org/10.1212/WNL.0b013e31824c4682>
- Pollock, N.S., M.E. Kargacin, and G.J. Kargacin. 1998. Chloride channel blockers inhibit Ca²⁺ uptake by the smooth muscle sarcoplasmic reticulum. *Biophys. J.* 75:1759–1766. [https://doi.org/10.1016/S0006-3495\(98\)77617-9](https://doi.org/10.1016/S0006-3495(98)77617-9)
- Samtleben, S., J. Jaepel, C. Fecher, T. Andreska, M. Rehberg, and R. Blum. 2013. Direct imaging of ER calcium with targeted-esterase induced dye loading (TED). *J. Vis. Exp.* (75):e50317. <https://doi.org/10.3791/50317>
- Sarkozy, A., D. Hicks, J. Hudson, S.H. Laval, R. Barresi, D. Hilton-Jones, M. Deschauer, E. Harris, L. Rufibach, E. Hwang, et al. 2013. ANO5 gene analysis in a large cohort of patients with anoctaminopathy: confirmation of male prevalence and high occurrence of the common exon 5 gene mutation. *Hum. Mutat.* 34:1111–1118. <https://doi.org/10.1002/humu.22342>
- Sharma, N., S. Medikayala, A. Defour, S. Rayavarapu, K.J. Brown, Y. Hathout, and J.K. Jaiswal. 2012. Use of quantitative membrane proteomics identifies a novel role of mitochondria in healing injured muscles. *J. Biol. Chem.* 287:30455–30467. <https://doi.org/10.1074/jbc.M112.354415>
- Sønder, S.L., T.L. Boye, R. Tölle, J. Dengjel, K. Maeda, M. Jäättelä, A.C. Simonsen, J.K. Jaiswal, and J. Nylandsted. 2019. Annexin A7 is required for ESCRT III-mediated plasma membrane repair. *Sci. Rep.* 9:6726. <https://doi.org/10.1038/s41598-019-43143-4>
- Stammers, A.N., S.E. Susser, N.C. Hamm, M.W. Hlynsky, D.E. Kimber, D.S. Kehler, and T.A. Duhamel. 2015. The regulation of sarco(endo)plasmic reticulum calcium-ATPases (SERCA). *Can. J. Physiol. Pharmacol.* 93: 843–854. <https://doi.org/10.1139/cjpp-2014-0463>
- Tsutsumi, S., N. Kamata, T.J. Vokes, Y. Maruoka, K. Nakakuki, S. Enomoto, K. Omura, T. Amagasa, M. Nagayama, F. Saito-Ohara, et al. 2004. The novel gene encoding a putative transmembrane protein is mutated in gnathodiaphyseal dysplasia (GDD). *Am. J. Hum. Genet.* 74:1255–1261. <https://doi.org/10.1086/421527>
- Tsutsumi, S., H. Inoue, Y. Sakamoto, K. Mizuta, N. Kamata, and M. Itakura. 2005. Molecular cloning and characterization of the murine gnathodiaphyseal dysplasia gene GDD1. *Biochem. Biophys. Res. Commun.* 331: 1099–1106. <https://doi.org/10.1016/j.bbrc.2005.03.226>
- Verkhatsky, A. 2005. Physiology and pathophysiology of the calcium store in the endoplasmic reticulum of neurons. *Physiol. Rev.* 85:201–279. <https://doi.org/10.1152/physrev.00004.2004>
- Vila, M.C., S. Rayavarapu, M.W. Hogarth, J.H. Van der Meulen, A. Horn, A. Defour, S. Takeda, K.J. Brown, Y. Hathout, K. Nagaraju, and J.K. Jaiswal. 2017. Mitochondria mediate cell membrane repair and contribute to

- Duchenne muscular dystrophy. *Cell Death Differ.* 24:330–342. <https://doi.org/10.1038/cdd.2016.127>
- Whitlock, J.M., and H.C. Hartzell. 2017. Anoctamins/TMEM16 Proteins: Chloride Channels Flirting with Lipids and Extracellular Vesicles. *Annu. Rev. Physiol.* 79:119–143. <https://doi.org/10.1146/annurev-physiol-022516-034031>
- Witting, N., M. Duno, H. Petri, T. Krag, H. Bundgaard, L. Kober, and J. Vissing. 2013. Anoctamin 5 muscular dystrophy in Denmark: prevalence, genotypes, phenotypes, cardiac findings, and muscle protein expression. *J. Neurol.* 260:2084–2093. <https://doi.org/10.1007/s00415-013-6934-y>
- Wu, J., L. Liu, T. Matsuda, Y. Zhao, A. Rebane, M. Drobizhev, Y.F. Chang, S. Araki, Y. Arai, K. March, et al. 2013. Improved orange and red Ca²⁺ indicators and photophysical considerations for optogenetic applications. *ACS Chem. Neurosci.* 4:963–972. <https://doi.org/10.1021/cn400012b>

Supplemental material

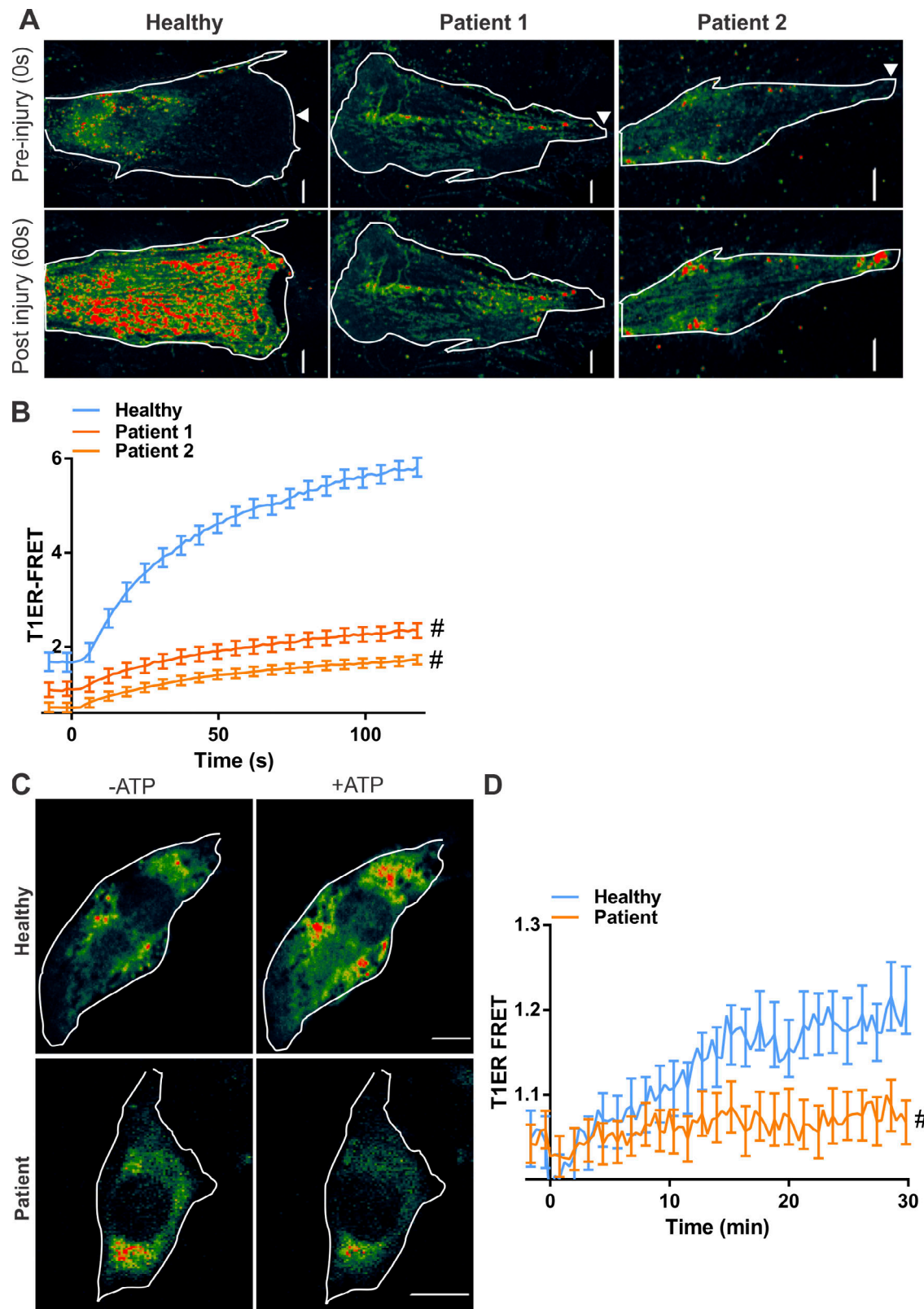


Figure S1. **ANO5 deficit reduces ER calcium uptake following purinergic stimulation. (A and B)** Healthy or ANO5-deficient patient fibroblasts expressing the ER calcium sensor T1ER were focally injured (arrowhead). Pseudocolored T1ER FRET images (A) and quantification (B) of normalized T1ER FRET, for cells before or following PM injury. $n = 17$ (healthy), 23 (patient 1), and 15 cells (patient 2). **(C and D)** Healthy or ANO5-deficient patient myoblasts expressing the ER calcium sensor T1ER were treated with ATP to induce Ca^{2+} entry into the cell. Pseudocolored T1ER FRET images (C) and quantification (D) of normalized T1ER FRET for cells before (-ATP) and 30 min following 50 μM ATP (+ATP) treatment. $n = 21$ (-ATP) and 17 cells (+ATP). Plots show mean \pm SEM. Scale bars, 10 μm . #, $P < 0.0001$.

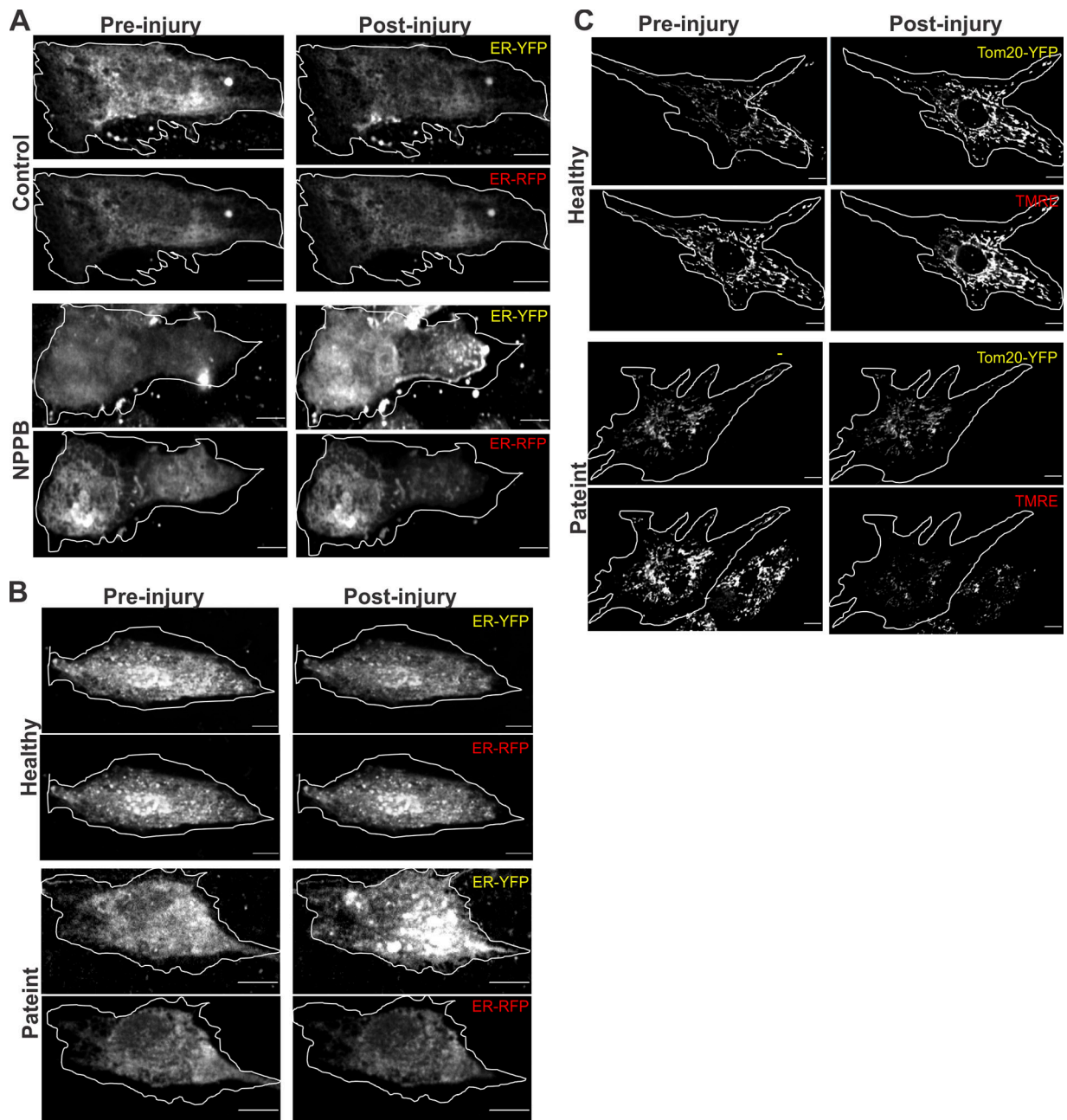


Figure S2. **Monochrome images of data presented in the main figures.** (A) Images accompanying Fig. 2 A. (B) Images accompanying Fig. 3 A. (C) Images accompanying Fig. 3 N. Scale bars, 10 μ m.

Downloaded from http://jcb.ingress.org/jcb/article-pdf/220/5/e202006035/1411452/jcb_202006035.pdf by INSERM user on 19 March 2021

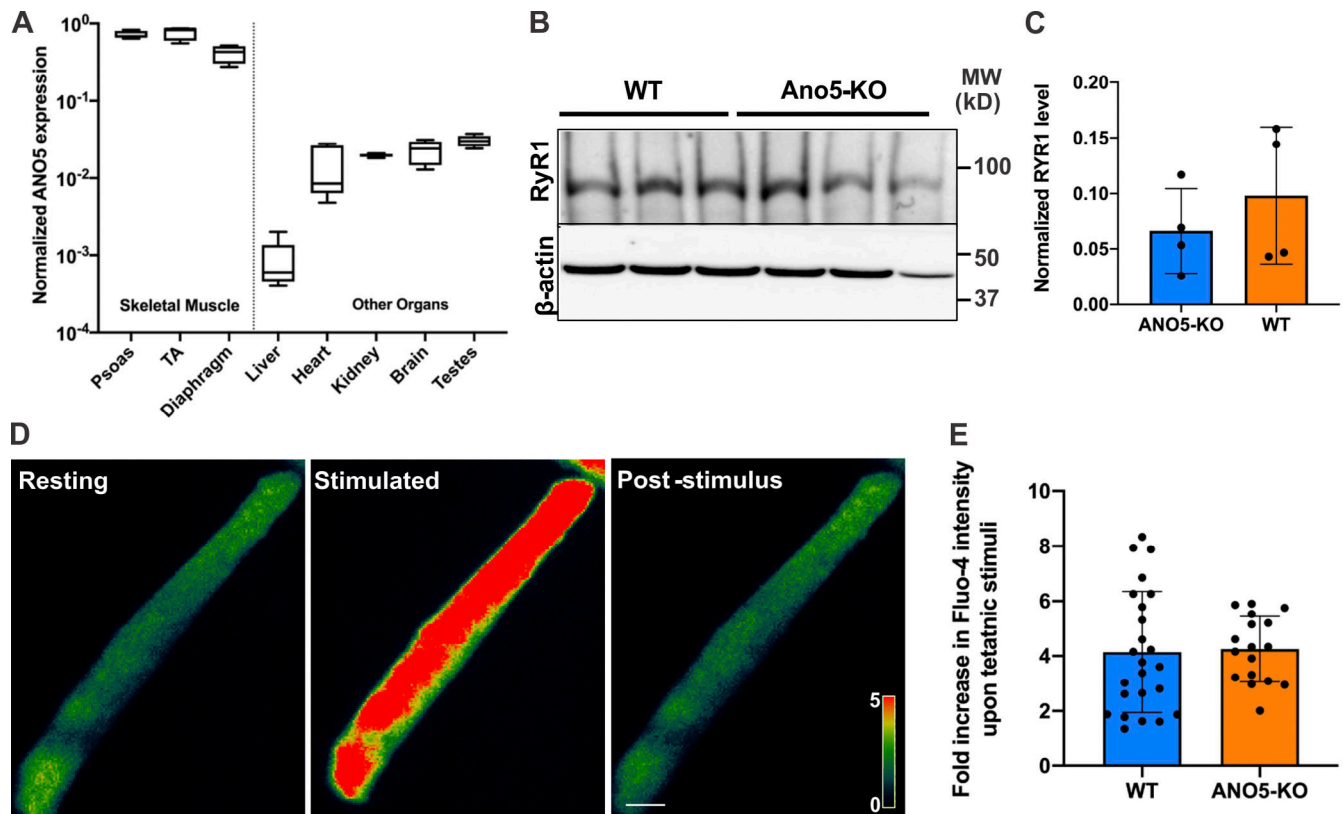


Figure S3. **ANO5 expression and effect of its deficit on the ER Ca²⁺-handling machinery.** (A) Quantitative PCR analysis of ANO5 mRNA expression in various mouse tissues. (B and C) Western blot showing a representative blot (B) and quantification (C) of RYR1 levels in tibialis anterior muscles from WT and ANO5-KO mice. (D and E) Pseudocolored images (D) and plot (E) showing an increase in FDB myofiber Ca²⁺ levels in WT and ANO5-KO mice using Fluo-4 dye. Plots show mean ± SD.